Late Oligocene Precipitation Seasonality in East Asia Based on $\delta^{13}C$ Profiles in Fossil Wood

J. R. Vornlocher[1†], W. E. Lukens[2], B. A. Schubert[1], and C. Quan[3]

[1]School of Geosciences, University of Louisiana at Lafayette, Lafayette, LA, 70504. [2]Department of Geology and Environmental Science, James Madison University, Harrisonburg, VA 22807. [3]School of Earth Science and Resources, Chang'an University, Xi'an, 710054, China

Corresponding author: William E. Lukens (lukenswe@jmu.edu)

†Current address: Department of Geology and Environmental Science, University of Pittsburgh, Pittsburgh, PA 15260.

Key Points:

- A seasonal rainfall proxy using tree rings $\delta^{13}C$ profiles was validated using living trees and weather station records in southern China
- Late Oligocene fossil tree ring $\delta^{13}C$ variations were consistent with rainfall levels ~4x higher in summer than winter
- Results suggest evidence for an East Asian Monsoon-style system in the Late Oligocene

Abstract

The wet summers and dry winters of monsoon systems in East Asia are a first-order control on food and water security for a significant portion of the global population today. The onset, characteristics, and drivers of paleo-monsoonal conditions in East Asia, however, are debated. Records from the Eocene suggest pronounced rainfall seasonality consistent with monsoon rainfall across China, likely driven by migrations of the Inter-Tropical Convergence Zone. Model simulations indicate that modern-like monsoon circulation of China was established by the early Miocene at the latest, but uncertainty remains due to a paucity of proxy records from the Oligocene. Here we provide the first annually resolved, quantitative estimates of precipitation from East Asia during the Oligocene, based upon intra-annual variation in carbon isotopes across growth rings of exquisitely preserved fossil wood from southern China. We find a clear pattern of consistent, summer-dominated precipitation with ~4 times more precipitation in summer than winter. These data demonstrate that by the late Oligocene, precipitation patterns in East Asia had similar strength and seasonality to modern conditions, which suggests the presence of an East Asian Monsoon-style system prior to the Neogene.

Plain Language Summary

The seasonal rainfall patterns of Asian monsoon systems affect food and water security for a substantial portion of global population. Prediction of monsoon behavior under warming climate conditions can be aided by studies of monsoon dynamics from ancient warm intervals, such as the Late Oligocene (~25 million years ago). We applied a novel technique to reconstruct rainfall patterns in southern China using high-resolution stable carbon isotope profiles in incredibly well preserved fossil wood. To demonstrate the robustness of this approach, we first validated the method using living trees and a nearby weather station. We then applied this method to fossil wood from the Late Oligocene. Our results suggest that summer rainfall (May-October) was ~4 times more than winter rainfall (November-April), which is indistinguishable from modern conditions in southern China. We conclude that the East Asian monsoon system was as strong as it is today during its very early stages in the Oligocene.

1 Introduction

The Cenozoic evolution of Asian monsoon systems remains a rich topic of debate and active, interdisciplinary investigation. Paleoclimate proxies and simulations suggest that highly seasonal precipitation existed across southern Asia in the Eocene, likely driven by migrations of the Inter-Tropical Convergence Zone (ITCZ) similar to the modern South Asian Monsoon or Indonesian-Australian Monsoon systems (Spicer et al., 2016; Li et al., 2018; Farnsworth et al., 2019; Tardif et al., 2020). A key feature of this early to middle Paleogene climate pattern is a west-east arid belt spanning much of China (Sun and Wang, 2005) that was possibly driven by the presence of a persistent high pressure system over central Asia (Tardif et al., 2020). This pattern differs from the modern East Asian Monsoon (EAM), which involves an incursion of moist air that penetrates deep into China and therefore disrupts a zonal precipitation gradient (Wang and LinHo, 2000). The timing of EAM initiation remains debated, ranging from the Eocene (Quan et al., 2012; Xie et al., 2019) to the late Oligocene (Sun and Wang, 2005) and Miocene (Clift et al., 2008; Liu et al., 2017; Spicer et al., 2017; Farnsworth et al., 2019). We contend that a key driver of this disagreement arises from a paucity of proxy records from East Asia during the Oligocene, compared to the Eocene and Miocene.

Precipitation seasonality and variability are intrinsic to monsoon systems; however, the majority of paleoclimate proxies applied to paleo-monsoon systems reconstruct mean annual conditions averaged across long timescales (decades to 10^5 years), large geographic areas, or offer qualitative interpretations of monsoon strength and pattern. The presence and characteristics of paleo-monsoons have been inferred indirectly through sedimentology (Loope et al., 2001; Licht et al., 2014), the stable isotope composition of paleosols (Quade et al., 1989; Zhisheng et al., 2005; Passey et al., 2009; Suarez et al., 2011), soil and rock magnetics (Liu et al., 2007; Yancheva et al., 2007), cosmogenic radionuclides (Beck et al., 2018), and paleobotanical proxies (Quan et al., 2012; Spicer et al., 2016, 2017; Xie et al., 2019, 2020). High-resolution isotope analysis on corals (Pradeep K. Aggarwal et al., 2004; Su et al., 2010), speleothems (Fleitmann et al., 2003; Cheng et al., 2016; Kathayat et al., 2017), gastropods (Licht et al., 2014), and mammal tooth enamel (Licht et al., 2014) can record intra- to inter-annual paleoclimate patterns. However, coral and speleothem records are only available for the Quaternary Period, and no model exists to quantitatively link annual isotope variations in shells or teeth to seasonal precipitation levels. Recent schlerochronological analyses from Paratetethys Sea oysters coupled with numerical model simulations have provided some of the first high resolution, seasonal paleoclimate reconstructions from the Eocene of central Asia and support interpretations of strongly seasonal precipitation over the region prior to the Neogene (Bougeois et al., 2014, 2018). While these marine paleoclimate proxies offer a substantial contribution to understanding the seasonal paleoclimatology of Asian monsoons, new terrestrial proxy records are needed for the Oligocene due to the closure of the Paratethys Sea at the end of the Eocene (van der Boon et al., 2018).

Here we present an annually resolved, quantitative reconstruction of summer and winter monsoon precipitation from southern China during the late Oligocene using stable carbon isotope measurements across growth rings of exquisitely preserved fossil wood, thus producing the first annual record of seasonal precipitation in East Asia from deep time. The late Oligocene Epoch of the Paleogene Period is an ideal time period for studying monsoon strength and variability because it post-dates major central Tibetan uplift (Fang et al., 2020) and coincides with the last time that CO_2 levels were consistently at least as high as today (Foster et al., 2017; Cui et al., 2020); however, paleoprecipitation records from the Oligocene in East Asia are rare. This new paleoclimate record will fill a key gap in proxy records from a region where billions of people rely on accurate forecasts of current and future monsoon dynamics.

2 Materials and Methods

2.1 Fossil and Living Trees

Three fossil wood specimens were selected for analysis from the Santang Konservat Lagerstätte, a newly described fossil plant assemblage (Quan et al., 2016; Huang et al., 2018; Ying et al., 2018). The taxonomic affinity of these fossils have been described previously by Huang et al. (2018), who observed traits in fossil specimens to be consistent with Castanopsis sp., a genus in the Fagaceae family with evergreen habit that lives today in tropical to subtropical East and Southeast Asia. Wood specimens of the fossil assemblage are stored and fully accessible in the Biological Museum of Sun Yat-sen University, Guangzhou, China.

The Santang fossil assemblage is preserved within a single lacustrine deposit of the upper Yongning Formation in Nanning Basin, Guangxi, China (22.881° N, 108.417° E, elevation = 83

m) (Fig. 1A-B) (Quan et al., 2016). The site is dated to late Oligocene based on *Anthracotherium changlingensis*, *Anthracokeryx kwangsiensis*, and *Heothema* mammal fossil assemblages within the upper Yongning Formation (Zhao, 1993; Ying et al., 2018), and independently supported by palynofloral analysis (Wang et al., 2015). Three fossil wood samples (NNW010, NNW12B, and NNW021, Fig. 1F-H) were selected for intra-ring $\delta^{13}C$ analysis in this study. Each ring was subdivided by hand using a razor blade perpendicular to the growth axis (Schubert and Jahren, 2011). A total of 20 rings were sampled (n = 518 slices).

We also studied two radial cores of evergreen trees living nearby the fossil assemblage (Pinus massoniana; samples QXS21A and QXS24A, Fig. 1D-E). Tree cores were extracted with an increment borer in 2016 at Qingxiushan Hill, Nanning, Guangxi, China (22.790 °N, 108.384 °E, elevation = 223 m, Fig. 1B). These trees were selected to test the seasonal precipitation proxy on extant evergreen trees growing in a monsoon-affected climate (Fig. 1C). Consecutive growth rings spanning the years 1990 to 2000 were sampled in an identical manner to the fossil wood. A total of 317 slices were collected from the two cores.

2.2 Stable Isotopes and Data Analysis

For modern and fossil samples, bulk wood slices weighing between 80-150 µg were wrapped in tin capsules for $\delta^{13}C$ analysis. Cellulose was not extracted for these data; our previous work has shown a robust linear correlation between the $\delta^{13}C$ value recorded in bulk wood tissue and α-cellulose (Lukens et al., 2019a), and the goal of our current study was to analyze relative changes in $\delta^{13}C$ value rather than exact values (after Schubert and Jahren, 2011). All $\delta^{13}C$ values were determined using a Thermo Finnigan Elemental Analyzer (Flash EA 1112 Series, Bremen, Germany) coupled with a Delta V Advantage Isotope-ratio Mass Spectrometer (Thermo Fisher) at the University of Louisiana at Lafayette. Samples were analyzed with three internal laboratory reference materials (JGLY, $\delta^{13}C$ = -43.51‰; JHIST, $\delta^{13}C$ = -8.13‰; JGLUC, $\delta^{13}C$ = -10.52‰). A quality assurance sample (JRICE, $\delta^{13}C$ = -27.44‰) was analyzed as an unknown with each batch run, and yielded a <0.1‰ analytical uncertainty. Isotope values are reported in δ-notation (‰) with respect to Vienna Pee Dee Belemnite (VPDB).

All statistical analyses were performed in RStudio version 3.6.1 (R Core Team, 2020).

2.3 Seasonal precipitation reconstruction

We reconstructed the ratio of seasonal, 6-month summer (P_s: May through October) and winter (P_w: November through April) precipitation in the Nanning Basin by applying a model developed by Schubert and Jahren (2011) to the intra-ring $\delta^{13}C$ analyses from modern and Oligocene trees. This proxy was calibrated using a global dataset of intra-ring $\delta^{13}C$ records from 33 angiosperm and gymnosperm trees growing across a range of environments (15 total sites), including southeast Asia. We note that other modern and fossil applications of this seasonal precipitation proxy have confirmed its utility for reconstructing seasonal rainfall across a wide latitudinal range (tropic to polar regions) and low or high seasonality (Schubert et al., 2012; Schubert and Timmermann, 2015; Schubert et al., 2017; Judd et al., 2019).

The model relates the amplitude of $\delta^{13}C$ values within a ring (H) to the annual variation in $\delta^{13}C$ of atmospheric CO_2 [$\Delta(\delta^{13}C_{CO2})$] and the ratio of P_w to P_s:

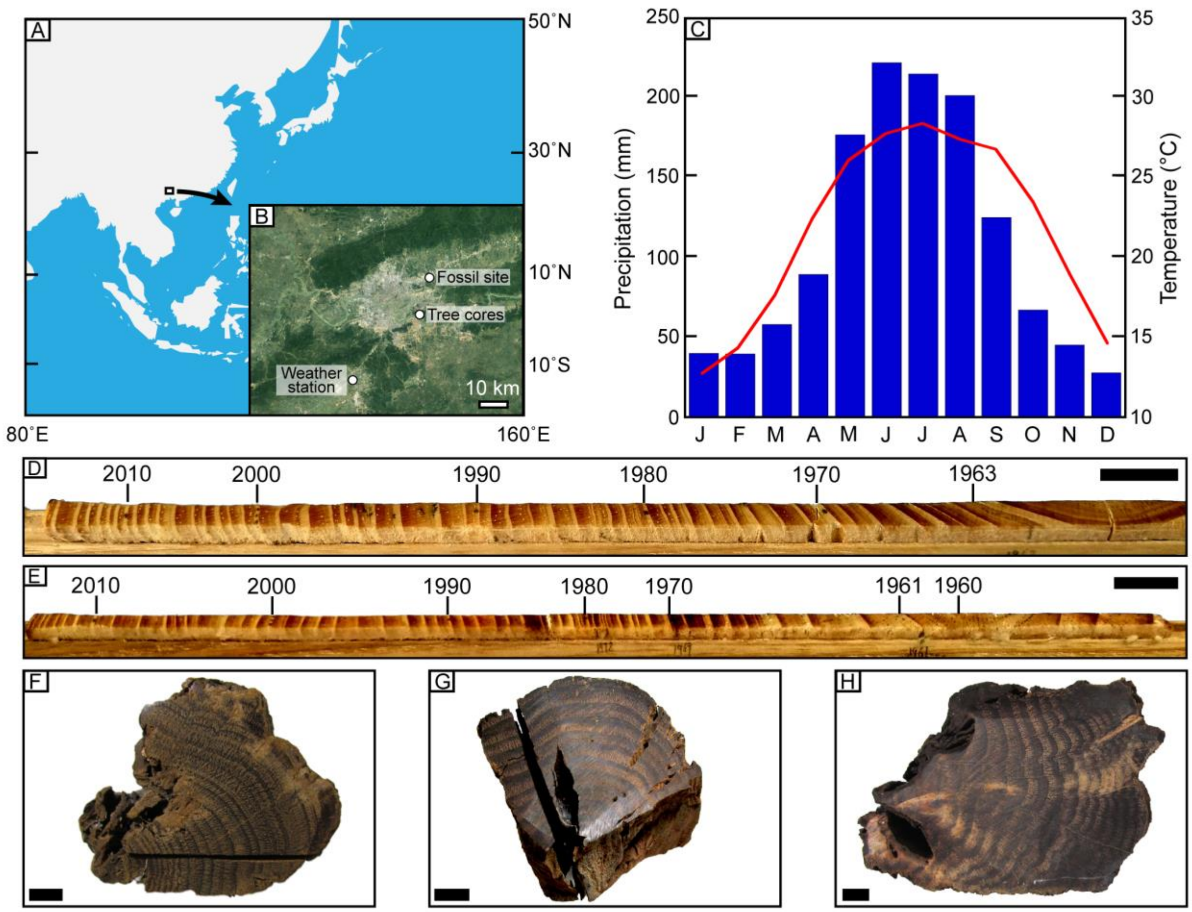

Figure 1. Location map and samples collected within the Nanning Basin, southern China (A). B) Locations of the modern tree cores, the local weather station (China Meteorological Data Service Center, Station No. 59431, http://data.cma.cn/), and fossil trees at the Santang Konservat Lagerstätte. Imagery courtesy of USGS/NASA Landsat via Google Earth. (C) Average monthly precipitation (blue bars) and temperature (red line) for Nanning, China (1951-2016 C.E.). D-E) Photographs of the modern *Pinus massoniana* tree cores QXS21A (top) and QXS24A (bottom). Growth direction is to the left. Years are labeled for reference. F-H) Photographs of the fossil evergreen wood samples used for this study: F) NNW010, G) NNW12B, and H) NNW021. For each wood sample, earlywood occurs as light bands and latewood occurs as subsequent dark bands. All black scale bars = 1 cm.

$$H = \Delta(\delta^{13}C_{CO2}) - 0.82[\ln(P_w/P_s)] + 0.73 \quad (1)$$

For the northern hemisphere, the empirical relationship between latitude and $\Delta(\delta^{13}C_{CO2})$ is:

$$\Delta(\delta^{13}C_{CO2}) = 0.01L + 0.13 \quad (2)$$

To adapt this model (Eq. 1) to the Nanning Basin $\delta^{13}C$ records, we substituted Eq. 2 in Eq. 1 and solved for P_w (see Supplement for full derivation):

$$P_w = (R)*(P_{total}) / (1 + R) \quad (3)$$

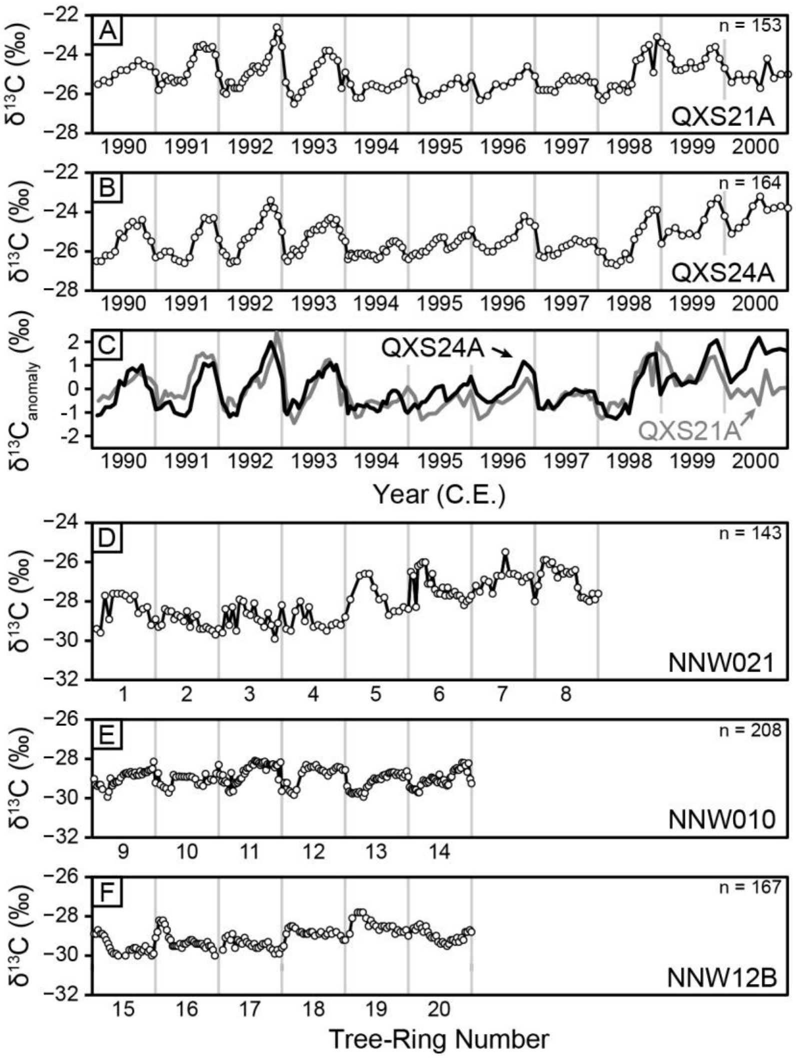

Figure 2. Profiles of $\delta^{13}C$ values across modern (A-C) and fossil wood (D-F). A-B) $\delta^{13}C$ profiles across modern *Pinus massioniana* tree cores. C) $\delta^{13}C$ profiles normalized to the average of each sample. D-F) $\delta^{13}C$ profiles across fossil evergreen wood; note that each profile represents a different fossil, and consequently rings are not correlated across the three fossil specimens. Gray vertical lines indicate ring boundaries. Number of analyses (n) is indicated in upper right of each panel; sample name is indicated in lower right of each panel.

$$P_s = P_w + P_{total} \qquad (4)$$

where

$$R = e\text{^}[(H + 0.01L – 0.6) / -0.82] \qquad (5)$$

Within Eq. 3-5, P_{total} is total annual precipitation, e is a mathematical constant (~2.718), H is the difference between the maximum $\delta^{13}C$ value of a given year and the preceding minimum $\delta^{13}C$ value of the annual cycle (after Schubert and Jahren, 2011), and L is latitude (22.8°N for modern Nanning).

3 Results

3.1. Development of high-resolution $\delta^{13}C$ profiles

The $\delta^{13}C$ values of the two modern *P. massoniana* tree cores differed significantly across the entire 1990-2000 series (Wilcoxon rank sum test, $p < 0.001$) (Fig. 2A-B), which is common for neighboring modern trees, even of the same species (e.g., Leavitt and Long, 1984). However, normalized $\delta^{13}C$ records of the modern wood showed the relative changes in $\delta^{13}C$ value to be consistent across individuals (Fig. 2C). On average, the late Oligocene wood fossils had significantly lower $\delta^{13}C$ values than the modern wood (Kruskall-Wallis rank sum test, $p < 0.001$) (Fig. 2D-F), consistent with preferential preservation of lignin relative to cellulose (Lukens et al., 2019a) and higher atmospheric CO_2 levels in the Oligocene relative to today (Schubert and Jahren, 2012; Foster et al., 2017). Notably, the fossil wood showed a similar quasi-periodic intra-ring $\delta^{13}C$ pattern to the modern wood, consistent with the evergreen habit inferred for the specimens based on previous work (Schubert and Jahren, 2011; Huang et al., 2018). Further, the amplitude of varying $\delta^{13}C$ values across each ring was not statistically different between the modern and fossil tree-rings (Kruskall-Wallis rank sum test, $p = 0.27$).

We used equations (1-3) to compare P_s and P_w calculated from the $\delta^{13}C$ pattern measured in the modern wood to the local climate station record (Fig. 2A-B; Table 1). We found a strong correlation between the climate station values and modeled P_s and P_w (Fig. 3; Pearson's $r = 0.92$) across the entire study period (1990-2000), confirming that the high-resolution $\delta^{13}C$ profiles accurately record the inter-annual variability in P_s and P_w at the site.

3.2 Comparison between Modern and Fossil Wood Isotope Data

The intra-ring patterns of $\delta^{13}C$ used for calculating seasonal precipitation were compared between modern and fossil wood samples. Median and standard deviations of H for the three fossils were as follows: NNW021 = 2.0 ± 0.7‰, NNW010 = 1.5 ± 0.2‰, and NNW12B = 1.4 ± 0.5‰. Median and standard deviations of H for the cores from the two living tress are as follows: QXS21A = 1.5 ± 0.9‰ and QXS24A = 1.9 ± 0.7‰. The Kruskall-Wallis rank sum test run on these data resulted in no significant difference between mean ranks (chi-square = 5.1517, degrees of freedom = 4, $p = 0.27$).

3.3 Late Oligocene Precipitation Reconstruction

We used the intra-ring $\delta^{13}C$ profiles measured across the fossil wood to estimate late Oligocene P_s and P_w via a Monte Carlo resampling that incorporates the normally distributed uncertainties associated with each of the dependent variables in equations (1-3). We estimated a conservative 1σ error of ± 10% for H values given that Schubert and Jahren (2011) found that an average of ~10 $\delta^{13}C$ measurements per growth ring obtains ~80% of the true H value. We set $P_{total} = 1296 \pm 227$ mm, which was the mean annual precipitation and standard deviation for the years 1951-2016 at the Nanning climate station. These values were supported for the late Oligocene based on pollen and plant macrofossils associated with the Nanning fossil wood deposit that were similar to extant flora in the area and were consistent with warm-temperate and humid conditions (Ying et al., 2018). Further, the presence of subhumid to humid climates interpreted for the now-arid interior of China during the late Oligocene indicated that southeast China was at least as wet (P_{total} > 1000 mm) (Miao et al., 2013). We note that because P_{total} is independent of P_w/P_s (equations S6 and S7), higher estimates of P_{total} serve to increase estimates of P_w and P_s, but proportionally, such that the ratio of P_w to P_s remains unchanged. In all cases, we found late Oligocene $P_s > P_w$ regardless of the P_{total} value. Because the South China Block has remained at or near its current latitude since the early Cenozoic (Wu et al., 2017), we used the modern latitude value (22.8^{o}N) with a conservative standard deviation of 5^o for late Oligocene paleolatitude. We found that changes of ± 5^o latitude affects calculated P_s and P_w values minimally.

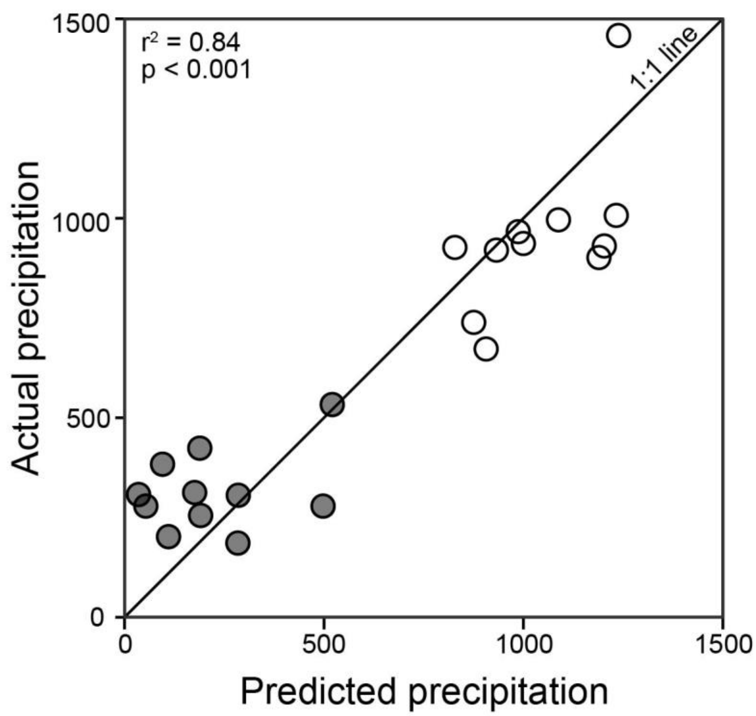

Figure 3. Validation of seasonal precipitation proxy. Winter precipitation (P_w: November through April; gray symbols) and summer precipitation (P_s: May through October; open symbols) are plotted against climate station records. Data are from 1990-2000 C.E. The H value from the two modern tree cores was averaged for each year prior to input into the model equations (1-5) (data for each core are reported in Table 1). Linear regression metrics are shown in upper left; diagonal line is a 1:1 line. Root mean square error is 140 mm.

Table 1. Climate and paleoclimate values for Nanning, China.

Sample	Year	P_{total}	P_w (observed)	P_s (observed)	H (‰)	Latitude (°N)	P_w (model)	P_s (model)
Modern tree cores and modern climate station data								
QXS24A	1990	1095	423	672	2.12	22.8	116	979
QXS24A	1991	1198	201	996	2.23	22.8	113	1085
QXS24A	1992	1238	307	931	3.18	22.8	39	1199
QXS24A	1993	1285	383	902	2.18	22.8	128	1157
QXS24A	1994	1736	279	1458	0.96	22.8	570	1167
QXS24A	1995	1272	306	966	1.54	22.8	247	1025
QXS24A	1996	1191	255	936	1.72	22.8	193	998
QXS24A	1997	1453	533	920	0.86	22.8	517	937
QXS24A	1998	1286	278	1007	2.69	22.8	72	1214
QXS24A	1999	1113	186	927	1.92	22.8	146	966
QXS24A	2000	1051	312	739	1.90	22.8	141	910
QXS21A	1990	1095	423	672	1.19	22.8	295	800
QXS21A	1991	1198	201	996	2.27	22.8	108	1090
QXS21A	1992	1238	307	931	3.36	22.8	32	1206
QXS21A	1993	1285	383	902	2.69	22.8	72	1213
QXS21A	1994	1736	279	1458	1.27	22.8	435	1301
QXS21A	1995	1272	306	966	1.24	22.8	328	944
QXS21A	1996	1191	255	936	1.73	22.8	191	1000
QXS21A	1997	1453	533	920	0.84	22.8	525	929
QXS21A	1998	1286	278	1007	3.21	22.8	39	1246
QXS21A	1999	1113	186	927	0.58	22.8	486	626
QXS21A	2000	1051	312	739	1.48	22.8	216	835
Late Oligocene tree cores and paleoclimate estimations								
NNW021	Ring1	1296	-	-	1.28	22.8	323	971
NNW021	Ring2	1296	-	-	0.88	22.8	453	840
NNW021	Ring3	1296	-	-	1.69	22.8	219	1074
NNW021	Ring4	1296	-	-	1.95	22.8	168	1125
NNW021	Ring5	1296	-	-	2.94	22.8	57	1236
NNW021	Ring6	1296	-	-	2.76	22.8	70	1223
NNW021	Ring7	1296	-	-	2.71	22.8	74	1219
NNW021	Ring8	1296	-	-	2.12	22.8	141	1152
NNW12B	Ring9	1296	-	-	1.85	22.8	186	1107
NNW12B	Ring10	1296	-	-	1.25	22.8	332	962
NNW12B	Ring11	1296	-	-	1.38	22.8	295	998
NNW12B	Ring12	1296	-	-	1.44	22.8	278	1015
NNW12B	Ring13	1296	-	-	0.60	22.8	558	736
NNW010	Ring14	1296	-	-	1.88	22.8	181	1112
NNW010	Ring15	1296	-	-	1.41	22.8	286	1007
NNW010	Ring16	1296	-	-	1.60	22.8	239	1054
NNW010	Ring17	1296	-	-	1.55	22.8	251	1043
NNW010	Ring18	1296	-	-	1.31	22.8	314	979
NNW010	Ring19	1296	-	-	1.52	22.8	258	1035

Note: Abbreviations are as follows. P_{total} = total precipitation, P_w = winter precipitation (November-April), P_s = summer precipitation (May-October), Actual = climate station-derived data, Model = proxy-derived estimates

We found that average late Oligocene P_s = 1058 ± 190 mm and P_w = 236 ± 55 mm (1σ error; n = 19 fossil rings) (Fig. 4A; Table 1). One sample (the first ring in sample NNW12B, labelled as ring 15 in Fig. 2) was omitted from analyses due to the peak $\delta^{13}C$ value occurring at the start of the ring. When calculating P_s and P_w for each fossil ring, we found that P_s was greater than P_w for all years, consistent with a summer-dominated precipitation regime for each of the years in which these trees grew during the late Oligocene. Further, these values were indistinguishable from present-day P_s and P_w measured at the local climate station (1000 ± 199 mm and 292 ± 99 mm, respectively; Fig. 4) and from model application on modern trees in Nanning, China (1044 ± 153 and 221 ± 164, respectively; Fig. 3). These results suggest that the strength and inter-annual variability of summer precipitation in the late Oligocene was similar to modern conditions, providing firm evidence for a strong monsoon. Using these results, we calculate conservative average summer rainfall rates during the late Oligocene of 5.8 ± 0.6 mm/day (with P_s = 82% of P_{total} on average), which closely matches present-day values at the site (5.5 ± 1.1 mm/day; P_s = 77% of P_{total} for 1951-2016). Because these daily rainfall rates represent 6-month averages, these values likely underestimate maximum daily rainfall rates during peak monsoon months. Nevertheless, these values exceed the threshold for monsoon climates defined by Wang and LinHo (2002)(≥3.0 mm/day and P_s ≥55% of P_{total}), and provide firm quantitative evidence for a paleo-monsoon using the metrics employed in modern climatology.

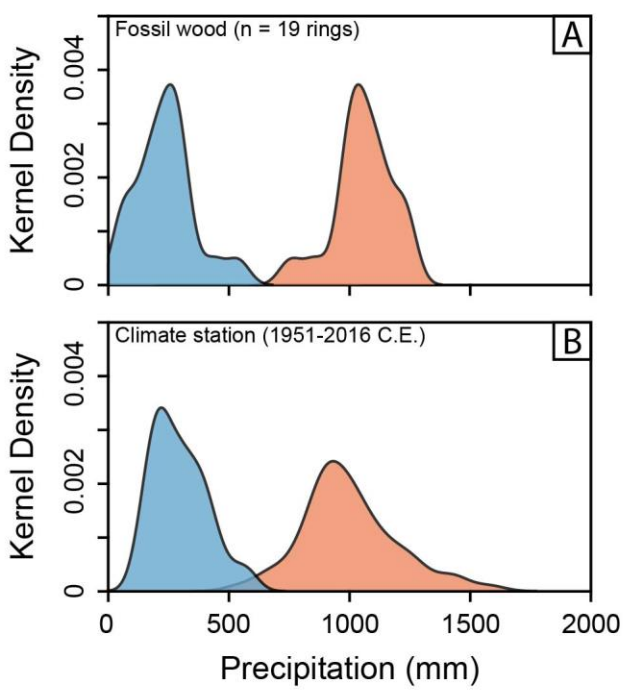

Figure 4. Kernel density functions plotted for winter precipitation (P_w, blue) and summer precipitation (P_s, red). A) Seasonal precipitation estimated from 19 fossil tree-rings. Note that P_s > P_w regardless of the P_{total} value input into equations (1-3) using the observed H values from the fossil tree-rings. B) Instrumental climate record for Nanning, China.

4 Discussion

Most studies that investigate monsoon systems in the geologic record focus on Quaternary records or rely on climate models to assess monsoon intensity and variability (Wang et al., 2017). Estimates of monsoon characteristics in deep-time using traditional mean annual precipitation (MAP) proxies such as stable isotopes in paleosols and fossil teeth (Passey, 2012), leaf morphometrics (Peppe et al., 2011), floral assemblages (Utescher et al., 2014), paleosol magnetics (Maxbauer et al., 2016), and paleosol bulk geochemistry (Stinchcomb et al., 2016; Lukens et al., 2019b), might be biased within monsoon regions that receive a large proportion of their annual precipitation within a few weeks or months, or during time intervals wherein spatial variability of isotopes in meteoric water may fundamentally alter isotope-precipitation relationships (e.g., Johnson and Ingram, 2004). These proxies can provide important information on long-term climate trends for a particular region (i.e., the EAM; Wang et al., 2019); however, they are unable to resolve inter- or intra-annual precipitation patterns that are characteristic of monsoon systems.

Our analyses of modern and fossil wood $\delta^{13}C$ profiles show similar overall patterns that are characteristic of evergreen trees growing in a strongly seasonal climate (Schubert and Jahren, 2011). This interpretation is supported by paleobotanical analyses from the Santang fossil assemblage by Huang et al. (2018). The wood fossils of the Fagaceae family have predominantly faint to absent growth rings, though some samples have distinct ring boundaries (such as those in this study; Fig. 1F-H). Importantly, though, some of the Castanopsis specimens in the fossil assemblage show indistinct growth ring boundaries with ring-porous patterns, which are features that have been observed in Castanopsis living today in Meghalaya, India (Sharma et al., 2011) and northern Thailand (Phromprasit et al., 2016). Both of these areas have strongly seasonal precipitation under the South Asian Monsoon. However, the Castanopsis fossils with distinct ring boundaries that lack ring porosity are possibly similar to those living in subtropical, EAM-affected areas of modern Japan, Taiwan and continental China (Huang et al., 2018). Collectively, the Santang wood fossils are therefore consistent with our interpretation of monsoon-style precipitation patterns in southern China during the late Oligocene.

A key input variable in the seasonal precipitation proxy used in this study is the annual cycle of $\delta^{13}C_{CO2}$ ($\Delta(\delta^{13}C_{CO2})$, Eq. 2). The slope and intercept of Eq. 2 are fitted to the modern pattern of annual variations in $\delta^{13}C_{CO2}$ value for the northern hemisphere, where $\Delta(\delta^{13}C_{CO2})$ increases with northing latitude. This relationship is driven by seasonal exchanges of C between the biosphere and atmosphere: photosynthesis in the boreal summer depletes the atmosphere in ^{12}C and enriches the remaining CO_2 in ^{13}C, followed by a wintertime release of ^{12}C back to the atmosphere as a result of soil respiration and reduced productivity (Keeling et al., 2005). The paleogeography of the Oligocene (e.g., Kennedy-Asser et al., 2019) suggests that northern hemisphere net primary productivity may have been enhanced relative to today, given 1) the lack of a permanent arctic ice cap, meaning more vegetation cover in the northern hemisphere and longer growing seasons, and 2) continent positions were largely similar to modern conditions. We tested the sensitivity of $\Delta(\delta^{13}C_{CO2})$ on seasonal precipitation estimates by varying this term in Eq. 1 from 0.0‰ (no annual change in $\delta^{13}C_{CO2}$) to 2.0‰ (twice the maximum possible value of $\delta^{13}C_{CO2}$ under modern conditions). Full details of this sensitivity analysis are provided in the Supplementary Materials. We found that for all measured H values, the ratio of estimated summer precipitation is little affected by an enhanced annual $\Delta(\delta^{13}C_{CO2})$ cycle (Fig. 5). We therefore conclude that our summer precipitation reconstructed values are robust.

Our results suggest that strong seasonality of rainfall in southern China may have been a feature of a late Oligocene, nascent EAM system. This conclusion is supported by recent work that shows evidence for a high central Tibetan Plateau (Fang et al., 2020) and a strong west-east hydroclimate gradient across Central Asia being established by the late Oligocene (Wang et al., 2020). Further, recent analyses of sporopollen populations across Chinese sedimentary basins are consistent with an EAM-style system arising in southern China starting as early as the middle Eocene (Xie et al., 2019, 2020) and strengthening through the late Oligocene (Sun and Wang, 2005).

5 Conclusions

The Oligocene remains a markedly understudied interval in monsoon paleoclimatology of southern and eastern Asia. The high-resolution $\delta^{13}C$ records from late Oligocene wood fossils presented in this study help to fill a critical gap in paleoprecipitation data from southern China. We report a robust record of summer-dominated rainfall for each of the 19 fossil rings we analyzed, consistent with 11 years of high resolution $\delta^{13}C$ profiles from living trees growing nearby. We suggest that these patterns indicate the presence of an East Asian Monsoon-style system in the late Oligocene, but further work is needed to connect these rainfall seasonality reconstructions with mechanisms of monsoon systems.

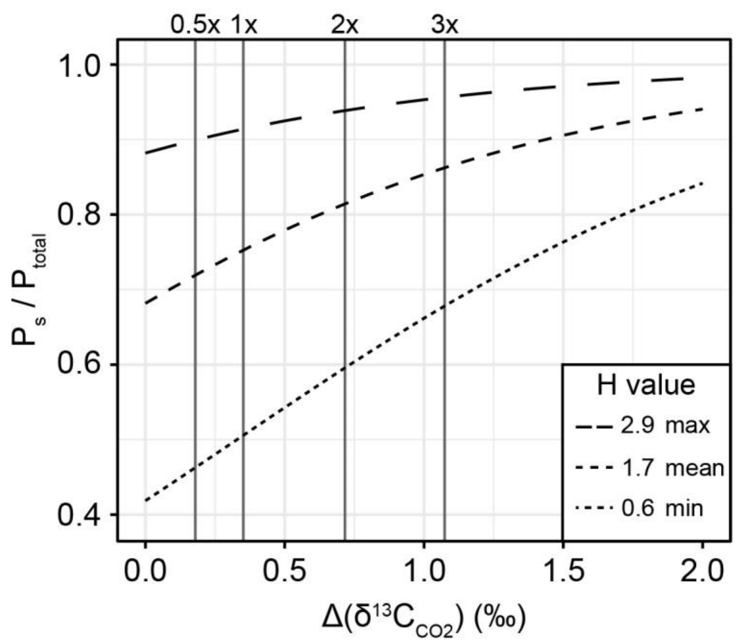

Figure 5. The fraction of summer precipitation to total annual precipitation (P_s/P_{total}) as a function of annual variation in atmospheric $\delta^{13}C_{CO2}$ value ($\Delta(\delta^{13}C_{CO2})$). The maximum, minimum, and mean H values for Nanning wood fossils are shown. At the modern latitude of Nanning, China (22.8 °N), the $\Delta(\delta^{13}C_{CO2})$ value is 0.35‰ (vertical line at 1x). Note that a doubling (2x) or tripling (3x) of this magnitude of $\delta^{13}C_{CO2}$ variation has relatively little effect and only increases estimates of summer rainfall proportions. Reduction of $\Delta(\delta^{13}C_{CO2})$ also has little effect the interpretation of late Oligocene summer-dominated rainfall.

Acknowledgments, Samples, and Data

We thank Dr. Yingfeng Xu for laboratory assistance and Dr. Keyan Fang for providing modern Pinus massoniana wood samples. This research was supported by U.S. National Science Foundation grant no. AGS-1903601. Fieldwork was supported by Natural Science Foundation of China nos. 41820104002 and 41888101. Datasets for this research are available in the Supplementary Information and also at https://doi.pangaea.de/10.1594/PANGAEA.919141.

References

Beck, J.W., Zhou, W., Li, C., Wu, Z., White, L., Xian, F., Kong, X., and An, Z., 2018, A 550,000-year record of East Asian monsoon rainfall from 10 Be in loess: Science (New York, N.Y.), v. 360, p. 877.

van der Boon, A., Beniest, A., Ciurej, A., Gaździcka, E., Grothe, A., Sachsenhofer, R.F., Langereis, C.G., and Krijgsman, W., 2018, The Eocene-Oligocene transition in the North Alpine Foreland Basin and subsequent closure of a Paratethys gateway: Global and Planetary Change, v. 162, p. 101–119, doi:10.1016/j.gloplacha.2017.12.009.

Bougeois, L., De Rafélis, M., Reichart, G.-J., De Nooijer, L.J., Nicollin, F., and Dupont-Nivet, G., 2014, A high resolution study of trace elements and stable isotopes in oyster shells to estimate Central Asian Middle Eocene seasonality: Chemical geology, v. 363, p. 200–212.

Bougeois, L., Dupont-Nivet, G., de Rafélis, M., Tindall, J.C., Proust, J.-N., Reichart, G.-J., de Nooijer, L.J., Guo, Z., and Ormukov, C., 2018, Asian monsoons and aridification response to Paleogene sea retreat and Neogene westerly shielding indicated by seasonality in Paratethys oysters: Earth and Planetary Science Letters, v. 485, p. 99–110.

Cheng, H. et al., 2016, The Asian monsoon over the past 640,000 years and ice age terminations: Nature, v. 534, p. 640–646, doi:10.1038/nature18591.

Clift, P.D., Hodges, K.V., Heslop, D., Hannigan, R., Van Long, H., and Calves, G., 2008, Correlation of Himalayan exhumation rates and Asian monsoon intensity:, doi:10.1038/ngeo351.

Cui, Y., Schubert, B.A., and Jahren, A.H., 2020, A 23 my record of low atmospheric CO2: Geology,.

Fang, X., Dupont-Nivet, G., Wang, C., Song, C., Meng, Q., Zhang, W., Nie, J., Zhang, T., Mao, Z., and Chen, Y., 2020, Revised chronology of central Tibet uplift (Lunpola Basin): Science Advances, v. 6, p. eaba7298, doi:10.1126/sciadv.aba7298.

Farnsworth, A. et al., 2019, Past East Asian monsoon evolution controlled by paleogeography, not CO2: Science Advances, v. 5, p. eaax1697, doi:10.1126/sciadv.aax1697.

Fleitmann, D., Burns, S.J., Mudelsee, M., Neff, U., Kramers, J., Mangini, A., and Matter, A., 2003, Holocene Forcing of the Indian Monsoon Recorded in a Stalagmite from Southern Oman: Science, v. 300, p. 1737–1739, doi:10.1126/science.1083130.

Foster, G.L., Royer, D.L., and Lunt, D.J., 2017, Future climate forcing potentially without precedent in the last 420 million years: Nature communications, v. 8, p. 14845, doi:10.1038/ncomms14845.

Huang, L., Jin, J., Quan, C., and Oskolski, A.A., 2018, Mummified fossil woods of Fagaceae from the upper Oligocene of Guangxi, South China: Journal of Asian Earth Sciences, v. 152, p. 39–51, doi:10.1016/j.jseaes.2017.11.029.

Johnson, K.R., and Ingram, B.L., 2004, Spatial and temporal variability in the stable isotope systematics of modern precipitation in China: implications for paleoclimate reconstructions: Earth and Planetary Science Letters, v. 220, p. 365–377, doi:10.1016/S0012-821X(04)00036-6.

Judd, E.J., Ivany, L.C., DeConto, R.M., Halberstadt, A.R.W., Miklus, N.M., Junium, C.K., and Uveges, B.T., 2019, Seasonally Resolved Proxy Data From the Antarctic Peninsula Support a Heterogeneous Middle Eocene Southern Ocean: Paleoceanography and Paleoclimatology, v. 34, p. 787–799, doi:10.1029/2019PA003581.

Kathayat, G., Cheng, H., Sinha, A., Yi, L., Li, X., Zhang, H., Li, H., Ning, Y., and Edwards, R.L., 2017, The Indian monsoon variability and civilization changes in the Indian subcontinent: Science advances, v. 3, p. e1701296, doi:10.1126/sciadv.1701296.

Keeling, C.D., Piper, S.C., Bacastow, R.B., Wahlen, M., Whorf, T.P., Heimann, M., and Meijer, H.A., 2005, Atmospheric CO 2 and 13 CO 2 exchange with the terrestrial biosphere and oceans from 1978 to 2000: Observations and carbon cycle implications, *in* A history of atmospheric CO2 and its effects on plants, animals, and ecosystems, Springer, p. 83–113.

Kennedy-Asser, A.T., Lunt, D.J., Farnsworth, A., and Valdes, P.J., 2019, Assessing mechanisms and uncertainty in modeled climatic change at the Eocene-Oligocene transition: Paleoceanography and Paleoclimatology, v. 34, p. 16–34.

Leavitt, S.W., and Long, A., 1984, Sampling strategy for stable carbon isotope analysis of tree rings in pine: Nature, v. 311, p. 145–147, doi:10.1038/311145a0.

Li, X., Zhang, Z., Zhang, R., and Yan, Q., 2018, Do climate simulations support the existence of East Asian monsoon climate in the Late Eocene? Palaeogeography, Palaeoclimatology, Palaeoecology, v. 509, p. 47–57, doi:10.1016/j.palaeo.2017.12.037.

Licht, A. et al., 2014, Asian monsoons in a late Eocene greenhouse world: Nature, v. 513, p. 501–506, doi:10.1038/nature13704.

Liu, Q., Deng, C., Torrent, J., and Zhu, R., 2007, Review of recent developments in mineral magnetism of the Chinese loess: Quaternary Science Reviews, v. 26, p. 368–385, doi:10.1016/j.quascirev.2006.08.004.

Liu, X., Dong, B., Yin, Z.-Y., Smith, R.S., and Guo, Q., 2017, Continental drift and plateau uplift control origination and evolution of Asian and Australian monsoons: Scientific reports, v. 7, p. 40344, doi:10.1038/srep40344.

Loope, D.B., Rowe, C.M., and Joeckel, R.M., 2001, Annual monsoon rains recorded by Jurassic dunes: Nature, v. 412, p. 64–66, doi:10.1038/35083554.

Lukens, W.E., Eze, P., and Schubert, B.A., 2019a, The effect of diagenesis on carbon isotope values of fossil wood: Geology, v. 47, p. 987–991, doi:10.1130/G46412.1.

Lukens, W.E., Stinchcomb, G.E., Nordt, L.C., Kahle, D.J., Driese, S.G., and Tubbs, J.D., 2019b, Recursive partitioning improves paleosol proxies for rainfall: American Journal of Science, v. 319, p. 819–845.

Maxbauer, D.P., Feinberg, J.M., and Fox, D.L., 2016, Magnetic mineral assemblages in soils and paleosols as the basis for paleoprecipitation proxies: A review of magnetic methods and challenges: Earth-Science Reviews, v. 155, p. 28–48, doi:10.1016/j.earscirev.2016.01.014.

Passey, B.H., 2012, Reconstructing Terrestrial Environments Using Stable Isotopes in Fossil Teeth and Paleosol Carbonates: The Paleontological Society Papers, v. 18, p. 167–194, doi:10.1017/S1089332600002606.

Passey, B.H., Ayliffe, L.K., Kaakinen, A., Zhang, Z., Eronen, J.T., Zhu, Y., Zhou, L., Cerling, T.E., and Fortelius, M., 2009, Strengthened East Asian summer monsoons during a period of high-latitude warmth? Isotopic evidence from Mio-Pliocene fossil mammals and soil carbonates from northern China: Earth and Planetary Science Letters, v. 277, p. 443–452, doi:10.1016/j.epsl.2008.11.008.

Peppe, D.J. et al., 2011, Sensitivity of leaf size and shape to climate: global patterns and paleoclimatic applications: The New Phytologist, v. 190, p. 724–739, doi:10.1111/j.1469-8137.2010.03615.x.

Phromprasit, P., Vajrodaya, S., and Kermanee, P., 2016, Species identification of some Castanopsis (D.Don) Spach (Fagaceae) species from Northern Thailand using wood characteristics: Thai Forest Bulletin (Botany), v. 44, p. 88–100, doi:10.20531/tfb.2016.44.2.01.

Pradeep K. Aggarwal, Klaus Fröhlich, Kshitij M. Kulkarni, and Laurence L. Gourcy, 2004, Stable isotope evidence for moisture sources in the asian summer monsoon under present and past climate regimes: Geophysical Research Letters, v. 31, p. L08203- n/a, doi:10.1029/2004GL019911.

Quade, J., Cerling, T.E., and Bowman, J.R., 1989, Development of Asian monsoon revealed by marked ecological shift during the latest Miocene in northern Pakistan: Nature, v. 342, p. 163–166, doi:10.1038/342163a0.

Quan, C., Fu, Q., Shi, G., Liu, Y., Li, L., Liu, X., and Jin, J., 2016, First Oligocene mummified plant Lagerstätte at the low latitiudes of East Asia: Science China, v. 59, p. 445–448.

Quan, C., Liu, Y.-S. (Christopher), and Utescher, T., 2012, Eocene monsoon prevalence over China: A paleobotanical perspective: Palaeogeography, Palaeoclimatology, Palaeoecology, v. 365–366, p. 302–311, doi:10.1016/j.palaeo.2012.09.035.

R Core Team, 2020, R: A Language and Environment for Statistical Computing: Vienna, Austria, R Foundation for Statistical Computing.

Schubert, B.A., and Jahren, A.H., 2011, Quantifying seasonal precipitation using high-resolution carbon isotope analyses in evergreen wood: Geochimica et Cosmochimica Acta, v. 75, p. 7291–7303, doi:10.1016/j.gca.2011.08.002.

Schubert, B.A., and Jahren, A.H., 2012, The effect of atmospheric CO2 concentration on carbon isotope fractionation in C3 land plants: Geochimica et Cosmochimica Acta, v. 96, p. 29–43, doi:10.1016/j.gca.2012.08.003.

Schubert, B.A., Jahren, A.H., Davydov, S.P., and Warny, S., 2017, The transitional climate of the late Miocene Arctic: Winter-dominated precipitation with high seasonal variability: Geology, v. 45, p. 447–450, doi:10.1130/G38746.1.

Schubert, B.A., Jahren, A.H., Eberle, J.J., Sternberg, L.S.L., and Eberth, D.A., 2012, A summertime rainy season in the Arctic forests of the Eocene: Geology, v. 40, p. 523–526, doi:10.1130/G32856.1.

Schubert, B.A., and Timmermann, A., 2015, Reconstruction of seasonal precipitation in Hawai'i using high-resolution carbon isotope measurements across tree rings: Chemical Geology, v. 417, p. 273–278, doi:10.1016/j.chemgeo.2015.10.013.

Sharma, C.L., Sharma, M., Carter, M.J., and Kharkongor, B.M., 2011, Inter species wood variation of Castanopsis species of Meghalaya: Journal of the Indian Academy of Wood Science, v. 8, p. 124–129.

Spicer, R., Yang, J., Herman, A., Kodrul, T., Aleksandrova, G., Maslova, N., Spicer, T., Ding, L., Xu, Q., and Shukla, A., 2017, Paleogene monsoons across India and South China: Drivers of biotic change: Gondwana Research, v. 49, p. 350–363.

Spicer, R.A., Yang, J., Herman, A.B., Kodrul, T., Maslova, N., Spicer, T.E., Aleksandrova, G., and Jin, J., 2016, Asian Eocene monsoons as revealed by leaf architectural signatures: Earth and Planetary Science Letters, v. 449, p. 61–68.

Stinchcomb, G.E., Nordt, L.C., Driese, S.G., Lukens, W.E., Williamson, F.C., and Tubbs, J.D., 2016, A data-driven spline model designed to predict paleoclimate using paleosol geochemistry: American Journal of Science, v. 316, p. 746–777, doi:10.2475/08.2016.02.

Su, R., Sun, D., Chen, H., Chen, X., and Li, Z., 2010, Evolution of Asian monsoon variability revealed by oxygen isotopic record of middle Holocene massive coral in the northern South China Sea: Quaternary International, v. 213, p. 56–68, doi:10.1016/j.quaint.2009.04.006.

Suarez, M.B., Passey, B.H., and Kaakinen, A., 2011, Paleosol carbonate multiple isotopologue signature of active East Asian summer monsoons during the late Miocene and Pliocene: Geology, v. 39, p. 1151–1154, doi:10.1130/G32350.1.

Sun, X., and Wang, P., 2005, How old is the Asian monsoon system?—Palaeobotanical records from China: Palaeogeography, Palaeoclimatology, Palaeoecology, v. 222, p. 181–222.

Tardif, D., Fluteau, F., Donnadieu, Y., Le Hir, G., Ladant, J.-B., Sepulchre, P., Licht, A., Poblete, F., and Dupont-Nivet, G., 2020, The origin of Asian monsoons: a modelling perspective: Climate of the Past, v. 16, p. 847–865, doi:https://doi.org/10.5194/cp-16-847-2020.

Utescher, T., Bruch, A.A., Erdei, B., François, L., Ivanov, D., Jacques, F.M.B., Kern, A.K., Liu, Y.-S. (C)., Mosbrugger, V., and Spicer, R.A., 2014, The Coexistence Approach—Theoretical background and practical considerations of using plant fossils for climate quantification: Palaeogeography, Palaeoclimatology, Palaeoecology, v. 410, p. 58–73, doi:10.1016/j.palaeo.2014.05.031.

Wang, X. et al., 2020, The role of the westerlies and orography in Asian hydroclimate since the late Oligocene: Geology, v. 48, p. 728–732, doi:10.1130/G47400.1.

Wang, W.M., Chen, G.J., and Liao, W., 2015, Oligocene palynoflora from Nanning Basin in Guangxi and its palaeoenvironmental significance: Quat Sci, v. 35, p. 1–10.

Wang, B., and Ho, L., 2002, Rainy season of the Asian–Pacific summer monsoon: Journal of Climate, v. 15, p. 386–398.

Wang, H., Lu, H., Zhao, L., Zhang, H., Lei, F., and Wang, Y., 2019, Asian monsoon rainfall variation during the Pliocene forced by global temperature change: Nature Communications, v. 10, p. 1–8, doi:10.1038/s41467-019-13338-4.

Wang, P.X., Wang, B., Cheng, H., Fasullo, J., Guo, Z., Kiefer, T., and Liu, Z., 2017, The global monsoon across time scales: Mechanisms and outstanding issues: Earth-Science Reviews, v. 174, p. 84–121.

Xie, Y., Wu, F., and Fang, X., 2020, A major environmental shift by the middle Eocene in southern China: Evidence from palynological records: Review of palaeobotany and palynology, p. 104226.

Xie, Y., Wu, F., and Fang, X., 2019, Middle Eocene East Asian monsoon prevalence over southern China: Evidence from palynological records: Global and Planetary Change, v. 175, p. 13–26.

Yancheva, G., Nowaczyk, N.R., Mingram, J., Dulski, P., Schettler, G., Negendank, J.F.W., Liu, J., Sigman, D.M., Peterson, L.C., and Haug, G.H., 2007, Influence of the intertropical convergence zone on the East Asian monsoon: Nature, v. 445, p. 74–77, doi:10.1038/nature05431.

Ying, T., Shaw, D., and Schneider, S., 2018, Oligocene fossil assemblages from Lake Nanning (Yongning Formation; Nanning Basin, Guangxi Province, SE China): Biodiversity and evolutionary implications: Palaeogeography, Palaeoclimatology, Palaeoecology, v. 505, p. 100–119, doi:10.1016/j.palaeo.2018.05.033.

Zhao, Z.R., 1993, New anthracothere materials from the Palaeogene of Guangxi: Vertebrata Palasiatica, v. 31, p. 183–190.

Zhisheng, A. et al., 2005, Multiple expansions of C4 plant biomass in East Asia since 7 Ma coupled with strengthened monsoon circulation: Geology, v. 33, p. 705–708, doi:10.1130/G21423.1.